

Measurement of neutron capture on ^{48}Ca at thermal and thermonuclear energies

H. Beer

Institut für Kernphysik, Forschungszentrum Karlsruhe, P. O. Box 3640, D-76021 Karlsruhe, Germany

C. Coceva

ENEA, Via Don Fiammelli 2, I-40128 Bologna, Italy

P. V. Sedyshev, and Yu. P. Popov

Frank Laboratory of Neutron Physics, JINR, 141980 Dubna, Moscow Region, Russia

H. Herndl, R. Hofinger, P. Mohr, and H. Oberhummer

Institut für Kernphysik, Wiedner Hauptstr. 8-10, TU Wien, A-1040 Vienna, Austria

(March 6, 2018)

At the Karlsruhe pulsed 3.75 MV Van de Graaff accelerator the thermonuclear $^{48}\text{Ca}(n,\gamma)^{49}\text{Ca}$ (8.72 min) cross section was measured by the fast cyclic activation technique via the 3084.5 keV γ -ray line of the ^{49}Ca -decay. Samples of CaCO_3 enriched in ^{48}Ca by 77.87 % were irradiated between two gold foils which served as capture standards. The capture cross-section was measured at the neutron energies 25, 151, 176, and 218 keV, respectively. Additionally, the thermal capture cross-section was measured at the reactor BR1 in Mol, Belgium, via the prompt and decay γ -ray lines using the same target material. The $^{48}\text{Ca}(n,\gamma)^{49}\text{Ca}$ cross-section in the thermonuclear and thermal energy range has been calculated using the direct-capture model combined with folding potentials. The potential strengths are adjusted to the scattering length and the binding energies of the final states in ^{49}Ca . The small coherent elastic cross section of $^{48}\text{Ca}+n$ is explained through the nuclear Ramsauer effect. Spectroscopic factors of ^{49}Ca have been extracted from the thermal capture cross-section with better accuracy than from a recent (d,p) experiment. Within the uncertainties both results are in agreement. The non-resonant thermal and thermonuclear experimental data for this reaction can be reproduced using the direct-capture model. A possible interference with a resonant contribution is discussed. The neutron spectroscopic factors of ^{49}Ca determined from shell-model calculations are compared with the values extracted from the experimental cross sections for $^{48}\text{Ca}(d,p)^{49}\text{Ca}$ and $^{48}\text{Ca}(n,\gamma)^{49}\text{Ca}$.

PACS numbers: 25.40.Lw, 24.50.+g, 25.40.Dn

I. INTRODUCTION

For a long time it has been known that the solar-system abundances of elements heavier than iron have been produced by neutron-capture reactions [1]. However, neutron capture is also of relevance for abundances of isotopes lighter than iron especially for neutron-rich isotopes, even though the bulk of these elements has been synthesized by charged-particle induced reactions. The attempts to understand neutron-induced nucleosynthesis require as important ingredients the knowledge of neutron-capture rates. The influence of shell effects on neutron capture is one of the most interesting aspects of neutron capture, especially since neutron capture in the vicinity of magic numbers is often a bottleneck in neutron-induced nucleosynthesis. This is the case also in neutron capture on neutron-rich isotopes close to the magic proton and neutron numbers $Z = 20$ and $N = 28$, i.e., in the vicinity of the double-magic nucleus ^{48}Ca . The neutron capture for nuclei in this mass region is of relevance for the Ca-Ti abundance anomalies occurring in certain primitive meteorites [2–4].

Neutron-capture on the double-magic nucleus ^{48}Ca at thermal and thermonuclear energies is also of interest from the viewpoint of nuclear structure. This nucleus has an excellent closed-shell structure and the level density of the compound-nucleus ^{49}Ca at neutron-separation energy is very low [5]. In fact, no strong resonances have been observed for ^{49}Ca in (d,p)-reactions or beta-delayed neutron decay below 172 keV. The two small resonances at 19.3 keV and 106.9 keV have only been observed in neutron capture [6,7], but have not been found in β -delayed neutron decay [8,9] and in the (d,p)-reaction [5,10]. They are probably d -wave resonances with a very small spectroscopic strength. Therefore, it can be expected that the resonant compound-nucleus contribution for $^{48}\text{Ca}(n,\gamma)^{49}\text{Ca}$ can be neglected and that the non-resonant direct capture is the dominant reaction mechanism. This has also been verified in a previous direct-capture calculation of $^{48}\text{Ca}(n,\gamma)^{49}\text{Ca}$ [11].

Neutron capture on $^{48}\text{Ca}(n,\gamma)^{49}\text{Ca}$ has been measured previously at thermal [12] and thermonuclear energies [7,13]. This data basis appeared to us not yet sufficient. At thermal neutron energy the measurement has a relative large uncertainty of 15%. The measurement was carried out with a sample of low ^{48}Ca enrichment using a Moxon-Rae detector. The thermonuclear time-of-flight measurement [7] was only sensitive to resonance capture and in the activation measurement [13] only two values were determined, using a Maxwell neutron spectrum of $kT=25$ keV and a very broad spectrum from a few keV to 170 keV (average energy: 97 keV).

II. EXPERIMENTAL SETUP AND RESULTS FOR THERMAL NEUTRON CAPTURE

The capture cross-section at thermal energy was obtained by measuring with a Ge-crystal the intensity of gamma-rays emitted with known probability after neutron capture in ^{48}Ca . More precisely, our experimental method is based on the following considerations. In the measured spectrum of capture gamma-rays, the number of counts $A(E_\gamma)$ in a peak corresponding to a given energy E_γ can be expressed as a product of four terms:

$$A(E_\gamma) = N_{\text{inc}} p_a f(E_\gamma) \varepsilon(E_\gamma) \quad , \quad (1)$$

where N_{inc} is the total number of neutrons incident on the sample, p_a is the capture probability (per incident neutron) in ^{48}Ca , $f(E_\gamma)$ is the *a priori* known emission probability (per capture event) of the gamma-ray under consideration, and $\varepsilon(E_\gamma)$ is its probability of being detected. The dependence of $A(E_\gamma)$ on the sought cross section σ_γ is contained in the probability p_a . For a thin sample (as in our case), the effect of capture in other nuclides, and of scattering can be considered as a correction for which a very precise knowledge of the relevant cross sections is not needed. In practice, p_a can be assumed to be a known function of $n\sigma_\gamma$, where n is the thickness (atoms per barn) of ^{48}Ca .

The product $N_{\text{inc}} \varepsilon(E_\gamma)$ in Eq. (1) must be deduced from a separate measurement of the gamma spectrum from the standard reaction $^{35}\text{Cl}(n,\gamma)$, using the same experimental set-up. In this calibration run, with reference again to Eq. (1), the probability p_a can be calculated from the known capture cross-section of ^{35}Cl and from the total cross-section of all sample components. Values of f are known for several calibration lines in the range of interest [14]. Summarizing, thanks to supplementary information on the emission probability f and on the product $N_{\text{inc}} \varepsilon$, we can state that some selected peak areas of the $^{48}\text{Ca}(n,\gamma)$ spectrum are known functions of the capture cross-section.

We should like to point out that the merit of this method lies in its intrinsic ability of picking out only those capture events occurring in a given nuclide of the sample. In our experiment advantage was taken of the precisely known [15] emission probabilities $f(3084.54 \text{ keV})=0.921 \pm 0.010$ and $f(4071.9 \text{ keV})=0.070 \pm 0.007$. These gamma-rays are emitted after β^- decay of ^{49}Ca with a half life of 523s. Moreover, we observed prompt gamma-rays in ^{49}Ca , i.e., the ground state transition at 5142 keV and the two-step cascade at 3121 and 2023 keV. It is known [16] that the intensity sum of the primary ground state transition and of the cascade through the 2023 keV level is very close to 100%. Therefore, we could use also these prompt transitions in ^{49}Ca to deduce the capture cross-section.

The experiment was carried out at the BR1 reactor of the "Studiecentrum voor kernenergie", Mol (Belgium), at an experimental channel supplying a thermal neutron flux of about $5 \times 10^5 / (\text{cm}^2 \text{ s})$ on the sample. The experimental set-up is schematically shown in Fig. 1. The sample consisted of about 0.1 g of Calcium carbonate (CaCO_3) containing 77.87% enriched ^{48}Ca (Tables I and II). Carbonate powder was enclosed in a cylindrical teflon container with 0.6 cm inner diameter.

As shown in Fig. 1, all detectors were shielded with particular care by means of Boron carbide and metallic ^6Li . In fact the rate of scattered neutrons from the sample and its container was two orders of magnitude higher than the capture rate in ^{48}Ca . Gamma-rays emitted by the sample were detected in a 130 cm^3 coaxial Ge crystal (labelled Ge2 in Fig. 1), completely surrounded by a $30 \text{ cm} \times 30 \text{ cm}$ NaI(Tl) scintillator, by a planar Ge crystal on the front side, and by a coaxial Ge crystal on the rear. All three Ge crystals were mounted in the same cryostat, housed in an 8 cm diameter through-hole along the axis of the NaI(Tl) cylinder.

A very effective suppression of escape peaks and Compton tails was obtained by rejecting all pulses from the central Ge crystal in coincidence with at least one of the other detectors. The energy resolution (FWHM) at 3 MeV was 2.9 keV. In the calibration run, CaCO_3 was replaced by a 61.835 mg sample of Carbon hexachloride (C_2Cl_6) in a similar teflon container. Here knowledge of the capture cross-section of ^{35}Cl ($\sigma_\gamma = (43.6 \pm 0.4)$ barn) and of the total cross-section of the sample components Cl and C [17] allow a very precise calculation of the capture probability p_a . Emission probabilities $f(E_\gamma)$ of 24 measured lines between 0.5 and 8.6 MeV are known within 3% [14].

Using the above data, the product $N_{\text{inc}} \varepsilon$ for five energies of ^{49}Ca and ^{49}Sc lines (Fig. reff2) was calculated from the curve

$$N_{\text{inc}} \varepsilon = a_1 + a_2 E_\gamma^{-a_3} \exp(-E_\gamma/a_4) \quad , \quad (2)$$

where the four parameters a_1, \dots, a_4 were obtained by best fitting the 24 calibration points of the Chlorine spectrum. It was demonstrated [18] that expression (2) can reproduce very accurately the energy dependence of Ge-detector efficiencies over a wide range. In fact, in our fit we obtained a normalised chi-square value $\chi^2 = 1.1$. The measurement with the ^{48}Ca sample lasted 35 hours, while the calibration with ^{35}Cl took 15 hours.

In conclusion, from the measured counts under the full-energy peaks of three lines of ^{49}Ca and of two lines of ^{49}Sc , the following consistent set of data was obtained: $f(5142\text{ keV}) = 0.74 \pm 0.03$; $f(3121\text{ keV}) = f(2023\text{ keV}) = 0.23 \pm 0.01$, and $p_a = (1.632 \pm 0.032) \times 10^{-3}$. Finally, the capture cross-section for ^{48}Ca deduced from the above p_a value is

$$\sigma_\gamma = (0.982 \pm 0.046) \text{ barn} \quad .$$

The quoted error is comprehensive of a systematic 2.4% uncertainty in the enrichment of the ^{48}Ca sample. The results are summarized in Table II.

III. FAST CYCLIC ACTIVATION TECHNIQUE AND THERMONUCLEAR CAPTURE CROSS-SECTIONS

The thermonuclear measurements have been carried out at the Karlsruhe pulsed 3.75 MV Van de Graaff accelerator. The technique of fast cyclic activation has been described in detail in previous publications [19,20]. To gain statistics the frequent repetition of the irradiation and activity counting procedure which characterizes a cycle is essential. The time constants for each cycle which are chosen shorter than the fluctuations of the neutron beam and comparable or shorter than the decay rate λ of the measured isotope ^{49}Ca are the irradiation time t_b , the counting time t_c , the waiting time t_w (the time to switch from the irradiation to the counting phase) and the total time $T = t_b + t_w + t_c + t'_w$ (t'_w the time to switch from the counting to the irradiation phase). In the actual ^{48}Ca measurements the runs were partly carried out with $t_b = 49.58\text{ s}$, $t_c = 49.24\text{ s}$, and $T = 100\text{ s}$, partly with $t_b = 99.58\text{ s}$, $t_c = 99.24\text{ s}$, and $T = 200\text{ s}$. The waiting time is in both cases $t_w = 0.42\text{ s}$.

The accumulated number of counts from a total of n cycles, $C = \sum_{i=1}^n C_i$, where C_i , the counts after the i -th cycle, are calculated for a chosen irradiation time, t_b , which is short enough compared with the fluctuations of the neutron flux, is [19]

$$C = \epsilon_\gamma K_\gamma f_\gamma \lambda^{-1} [1 - \exp(-\lambda t_c)] \exp(-\lambda t_w) \frac{1 - \exp(-\lambda t_b)}{1 - \exp(-\lambda T)} N \sigma [1 - f_b \exp(-\lambda T)] \sum_{i=1}^n \Phi_i \quad (3)$$

with

$$f_b = \frac{\sum_{i=1}^n \Phi_i \exp[-(n-i)\lambda T]}{\sum_{i=1}^n \Phi_i} \quad .$$

The following additional quantities have been defined; ϵ_γ : Ge-efficiency, K_γ : γ -ray absorption, f_γ : γ -ray intensity per decay, N : the number of target nuclei, σ : the capture cross-section, Φ_i : the neutron flux in the i -th cycle. The quantity f_b is calculated from the registered flux history of a ^6Li glass monitor.

The efficiency determination of the 35% HPGe-detector (2 keV resolution at 1.332 MeV) has been reported elsewhere [21]. The γ -ray absorption was calculated using tables published by Storm and Israel [22] and Veigle [23]. The half-lives and the γ -ray intensities per decay of ^{49}Ca and ^{198}Au are given in Table I.

The activities of nuclides with half lives of several hours to days, i.e., the activity of ^{198}Au , is additionally counted after the end of the cyclic activation consisting of n cycles using

$$C_n = \epsilon_\gamma K_\gamma f_\gamma \lambda^{-1} [1 - \exp(-\lambda T_M)] \exp(-\lambda T_W) [1 - \exp(-\lambda t_b)] N \sigma f_b \sum_{i=1}^n \Phi_i \quad . \quad (4)$$

Here T_M is the measuring time of the Ge-detector and T_W the time elapsed between the end of cyclic activation and begin of the new data acquisition.

Eqs. (3) and (4), respectively, contain the quantities σ and the total neutron flux $\sum_{i=1}^n \Phi_i$. The unknown capture cross-section of ^{48}Ca is measured relative to the well-known standard cross section of ^{197}Au [24,25]. As the $^{48}\text{CaCO}_3$ sample to be investigated is characterized by a finite thickness it is necessary to sandwich the sample by two comparatively thin gold foils for the determination of the effective neutron flux at sample position. The activities of these gold foils were counted also individually after termination of the cyclic activation. The effective count rate of gold was obtained from these individual rates as well as from the accumulated gold count rate during the cyclic activation run.

Therefore, the effective neutron flux at sample position was determined in two ways by way of the gold activation according to the Eqs. (3) and (4). Using Eq. (3) has the advantage that saturation effects in the gold activity for irradiations over several days are avoided [19].

The neutron spectrum at the neutron energy 25 keV was generated using proton energies close to the reaction threshold. This condition produces a kinematically collimated neutron spectrum resembling a Maxwellian spectrum at a temperature of 25 keV. The spectra at 151, 176, and 218 keV were generated using thin Li-targets (2.5 μm). The required proton energy conditions and the neutron spectra integrated over the solid angle of the sample were determined in time-of-flight (TOF) measurements before the actual activation runs using the accelerator in pulsed mode. The measurements were carried out under the same conditions as previously reported for the $^{36}\text{S}(n,\gamma)^{37}\text{S}$ experiment [20]. Table III gives a survey of the sample weights and the measured ^{48}Ca capture cross-sections. The $^{48}\text{CaCO}_3$ sample of 6 mm diameter was sandwiched by thin gold foils of the same dimensions. At 25 keV neutron energy measurements were carried out with calcium carbonat sample masses between 7 and 70 mg. No significant effect from multiple neutron scattering was observed. A sample of the $^{48}\text{CaCO}_3$ powder was also heated to 300° C for 3 hours. A weight loss of only 0.45 % may be ascribed to absorbed water. In Fig. 3 the accumulated γ -ray intensity from one of the ^{48}Ca activations is shown. The γ -line is well isolated on a low level of background counts.

As it was very difficult to press the $^{48}\text{CaCO}_3$ powder to stable self supporting tablets, the material was in most cases filled into cylindrical polyethylene or teflon containers. When we succeeded to press a somewhat stable tablet it was put into a thin Al-foil. No measurable effects due to the containment were detected. As our measurements are significantly below an earlier measurement [13] especially at 25 keV neutron energy all these checks were performed. To be sure that the enrichment is correct an additional mass spectrometric analysis was carried out by the "Wiederaufarbeitungsanlage Karlsruhe (WAK)" which confirmed the original certificate. As the detector showed also radiation damage in the last runs, the efficiency was rechecked with radioactive samples. Finally, to the sandwich of gold foils a sandwich of Ag-foils was added in the run at 25 keV with the 7 mg $^{48}\text{CaCO}_3$ sample. If we relate in this run the ^{48}Ca cross-section to the previously measured capture cross sections of $^{107,109}\text{Ag}$ [19], we obtain $(855\pm 150)\mu\text{barn}$ which is indeed higher by 14 % but within quoted uncertainties agrees with our measurements related to the ^{197}Au capture cross-section.

The following systematic uncertainties were combined by quadratic error propagation; Au standard cross section: 1.5-3 %, Ge-detector efficiency: 8 %, γ -ray intensity per decay: 1.1 % for the ^{49}Ca and 0.1 % for the ^{198}Au decay, divergence of neutron beam: 2-7 %, factor f_b : 1.5 %, sample weight: <0.5 %, and other systematic errors: 3 %.

IV. CALCULATIONS AND RESULTS

Neutron capture on several calcium isotopes has been analyzed recently by Krausmann *et al.* [11] using the direct-capture (DC) model together with folding potentials. The DC formalism was developed by Kim *et al.* [26], and can also be found in [11,27]. Here we only repeat some relations which are important for the subsequent calculations.

The DC cross-section for the capture to a final state i is given by

$$\begin{aligned} \sigma_i^{\text{DC}} &= \int d\Omega \frac{d\sigma^{\text{DC}}}{d\Omega_\gamma} \\ &= \int d\Omega 2 \left(\frac{e^2}{\hbar c} \right) \left(\frac{\mu c^2}{\hbar c} \right) \left(\frac{k_\gamma}{k_a} \right)^3 \frac{1}{2 I_A + 1} \frac{1}{2 S_a + 1} \sum_{M_A M_a M_B, \sigma} |T_{M_A M_a M_B, \sigma}|^2 \quad . \end{aligned} \quad (5)$$

The quantities I_A , I_B and S_a (M_A , M_B and M_a) are the spins (magnetic quantum numbers) of the target nucleus A , residual nucleus B and projectile a , respectively. The reduced mass in the entrance channel is given by μ . The polarization σ of the electromagnetic radiation can be ± 1 . The wave number in the entrance channel and for the emitted radiation is given by k_a and k_γ , respectively. The total capture cross-section is given by the sum over all DC cross-sections for each final state i , multiplied by the spectroscopic factor C^2S which is a measure for the probability of finding ^{49}Ca in a ($^{48}\text{Ca} \otimes n$) single-particle configuration

$$\sigma^{\text{th}} = \sum_i C_i^2 S_i \sigma_i^{\text{DC}} \quad . \quad (6)$$

The transition matrices $T = T^{\text{E1}} + T^{\text{E2}} + T^{\text{M1}}$ depend on the overlap integrals

$$I_{l_b j_b I_B; l_a j_a}^{\text{EL/MC}} = \int dr U_{l_b j_b I_B}(r) \mathcal{O}^{\text{EL/MC}}(r) \chi_{l_a j_a}(r) \quad (7)$$

The radial part of the bound state wave function in the exit channel and the scattering wave function in the entrance channel is given by $U_{l_b j_b I_B}(r)$ and $\chi_{l_a j_a}(r)$, respectively. The radial parts of the electromagnetic multipole operators are well-known (e.g., [11]). The calculation of the DC cross-sections has been performed using the code TEDCA [28].

The most important ingredients in the potential models are the wave functions for the scattering and bound states in the entrance and exit channels. For the calculation of the wave functions we use real Saxon-Woods (SW) potentials as well as real folding potentials which are given by

$$V(R) = \lambda V_F(R) = \lambda \int \int \rho_a(\mathbf{r}_1) \rho_A(\mathbf{r}_2) v_{\text{eff}}(E, \rho_a, \rho_A, s) d\mathbf{r}_1 d\mathbf{r}_2 \quad (8)$$

with λ being a potential strength parameter close to unity, and $s = |\mathbf{R} + \mathbf{r}_2 - \mathbf{r}_1|$, where R is the separation of the centers of mass of the projectile and the target nucleus. The density of ^{48}Ca has been derived from the measured charge distribution [29], and the effective nucleon-nucleon interaction v_{eff} has been taken in the DDM3Y parametrization [30]. The resulting folding potential has a volume integral per interacting nucleon pair $J_R = 446.63 \text{ MeV fm}^3$ ($\lambda = 1$) and an rms-radius $r_{\text{rms}} = 4.038 \text{ fm}$. Details about the folding procedure can be found for instance in [31], the folding potential has been calculated by using the code DFOLD [32]. The imaginary part of the potential is very small because of the small flux into reaction channels [11] and can be neglected in our case.

Two important results have been obtained in the work of Kraussmann *et al.* [11]: first, the $^{48}\text{Ca}(n, \gamma)^{49}\text{Ca}$ reaction can be well described in terms of a direct-reaction mechanism, and second, only the E1-transitions from the incoming s-wave to the ground state of ^{49}Ca ($3/2^-$) and to the first excited state at $E^* = 2023 \text{ keV}$ ($1/2^-$) play a significant role in the thermal and thermonuclear energy range (Fig. 4).

The neutron scattering length on ^{48}Ca has been measured by Raman *et al.* [33]: $b = (0.36 \pm 0.09) \text{ fm}$. As can be seen from Fig. 5 (upper part), the optical potential can be adjusted very accurately to the scattering length or to the coherent scattering cross-section (which is given by $\sigma^{\text{coh}} = 4\pi b^2 = (16.3 \pm 8.1) \text{ mb}$), because even small changes in the strength of the potential result in drastic changes of the scattering length. For the folding potential we obtain $\lambda = 0.9712 \pm 0.0015$, and $J_R = (433.75 \pm 0.65) \text{ MeV fm}^3$, for a SW potential with standard geometry ($r_0 = 1.25 \text{ fm}$, $a = 0.65 \text{ fm}$) we obtain $V_0 = (47.74 \pm 0.08) \text{ MeV}$, and $J_R = (469.57 \pm 0.79) \text{ MeV fm}^3$. The folding potential has only one parameter λ which can be adjusted directly to the scattering length; the geometry of this potential is fixed by the folding procedure. This is a clear advantage compared to the usual SW potential, where one has to choose reasonable values for the radius parameter r_0 and the surface diffuseness a .

From Fig. 5 (central part) one notices that the value of the coherent ($n+^{48}\text{Ca}$)-scattering cross-section almost disappears for a volume integral near $J_R = 436 \text{ MeV fm}^3$. In fact, the experimental coherent elastic cross section for ($n+^{48}\text{Ca}$)-scattering (horizontal shaded area in the central part of Fig. 5) has by far the lowest value for all known target nuclei [34]. This is due to the so-called nuclear Ramsauer effect [35,36], which is analogous to the already long-known electron-atomic effect [37]. The condition for a minimum in the elastic cross section is that the phase-shift difference of the neutron paths traversing the nucleus and going around is $\Delta = n\pi$ with $n = \text{even}$ [36]. For low energies the phase shift for going outside the nucleus can be neglected so that the above expression reduces to $\delta = \Delta/2 = m\pi = n\pi/2$ with $m = \text{integer}$, where δ is now the normal scattering phase shift. As can be seen from the solid curve in Fig. 6 for the phase shift in ($n+^{48}\text{Ca}$)-scattering $m = n/2 = 2$. Almost the same scattering wave function in the nuclear exterior is obtained for a vanishing potential (broken curve in Fig. 6). That means that near zero neutron energy almost exactly two neutron-wavelengths ($m = 2$, $n = 4$) fit inside the ^{48}Ca nucleus, giving a pronounced minimum in the cross section.

This neutron-nuclear situation contrasts with the electron-atomic Ramsauer effect, where only one minimum ($m = 1$, $n = 2$) is possible. Elastic neutron scattering on ^{48}Ca is an excellent example for the nuclear Ramsauer effect, because neutron-induced low-energy absorption into other channels is (compared with other nuclei) exceptionally low [34]. This means that for elastic neutron scattering on ^{48}Ca also the elastic shadow scattering is very small. Both effects (nuclear Ramsauer effect, almost no absorption into other channels) lead to the extremely small cross section in elastic low-energy neutron scattering on ^{48}Ca .

The bound state wave functions are calculated using the same folding-potential shape as for the scattering waves. Only the potential strengths have been adjusted to reproduce the binding energies of the $3/2^-$ and $1/2^-$ bound states. The resulting parameters are listed in Table IV.

According to Eq. (6) spectroscopic factors C^2S of the two bound states can be extracted from the ratio of the measured thermal capture cross-section of the two final states and the calculated thermal DC cross-section. This can again be done with high accuracy because the calculated DC cross-section is not very sensitive to small changes of the strength of the optical potential (see lower part of Fig. 5). The resulting spectroscopic factors (see Table IV) depend only weakly on the chosen potential (folding potential or Saxon-Woods potential). The spectroscopic factors are somewhat smaller than values determined in a recent (d,p)-experiment but both values agree within their uncertainties which are smaller in this determination of C^2S compared to the extraction of C^2S from the analysis of a (d,p)-experiment (see Table IV).

For the calculation of the thermonuclear capture cross-section no parameters have to be adjusted to the experimental data. The optical potentials, bound state wave functions and spectroscopic factors have been determined from the scattering length and the thermal capture cross-section. In Fig. 7 the result of our calculation is compared to the experimental data available in literature [12,13] and to our new experimental data. Good agreement between the DC calculation and the experimental data is obtained.

Only our experimental value at a neutron energy of $E_n = 25$ keV is about 25 % lower compared to the calculated direct-capture cross-section as well as the one obtained from extrapolating the thermal cross section with an $1/v$ -behavior. This difference could be explained through a destructive interference of the direct part with a resonance having the parameters $E_{\text{res}} = 1.45$ keV, $\Gamma_n = 0.33$ keV, and $\Gamma_\gamma = 0.22$ eV. However, in the neutron-capture data taken at ORELA some years ago [6,7] such a strong resonance peak should have been observed [38]. The two small resonances at 19.3 keV and 106.9 keV that have been observed are much weaker than the proposed resonance.

In Table V the neutron spectroscopic factors of ^{49}Ca determined from shell-model calculations are compared with the values extracted from the experimental cross sections for $^{48}\text{Ca}(d,p)^{49}\text{Ca}$ and $^{48}\text{Ca}(n,\gamma)^{49}\text{Ca}$. This comparison of the experimental data with the calculated values is especially important as they form the basis for the extrapolation of the calculations of neutron capture on neutron-rich unstable target nuclei in the mass number range $A = 36$ to $A = 66$, where experimental data is scarcely or not at all available. However, the knowledge of these cross sections is an essential part in the explanation of the isotopic anomalies of Ca–Al-rich inclusions of certain primitive meteorites [39,40]. The cross sections and reaction rates must be calculated via the direct reaction model using the input data of nuclear structure models, for instance the shell model. The spectroscopic factors calculated in the shell model have been obtained using the code OXBASH [41]. We have employed the interaction FPD6 of Richter et al. [42] which assumes an inert ^{40}Ca -core and the remaining nucleons in the full fp-shell. As can be seen from Table V the spectroscopic factors agree well for the ground state, the first $1/2^-$ and the second $5/2^-$ state. These states are almost pure single particle states. The first $5/2^-$ and the second $1/2^-$ state cannot be reproduced with this interaction.

We have determined the thermonuclear-reaction-rate factor $N_A \langle \sigma v \rangle$ [43]. Since the cross section follows an $1/v$ -law up to at least 220 keV we obtain a constant reaction-rate factor

$$N_A \langle \sigma v \rangle = 1.28 \times 10^5 \text{ cm}^3 \text{ mole}^{-1} \text{ s}^{-1} \quad . \quad (9)$$

V. SUMMARY

We have measured the thermal and thermonuclear (25, 151, 176, and 218 keV) $^{48}\text{Ca}(n,\gamma)$ cross-sections. From these data we calculated the thermonuclear-reaction-rate factor. We found the thermal capture cross-section 10 % lower than the previous value of Cranston and White [12]. In the analysis our thermal cross section was found to be consistent with our thermonuclear values assuming a $1/v$ -behavior, except the 25 keV value which was lower by 25 %. The previous thermonuclear values of Käppeler et al. [13] are satisfactory compared with the fit to our experimental data. As anticipated by previous experimental results there is only negligible influence of the resonance part of the cross section up to at least 220 keV. Therefore, the neutron capture by ^{48}Ca can be well described in this case by using a direct-capture model.

ACKNOWLEDGEMENTS

We are grateful to Richard L. Macklin and Jack Harvey for giving us additional valuable information of their ^{48}Ca time-of-flight measurements. From the IRMM, Geel, we thank C. Van der Vorst and E. Macavero for their help in the thermal measurement at the reactor BR1 in Mol. The support of the BR1 reactor staff is also gratefully acknowledged. We would like to thank the technician of the Van de Graaff G. Rupp and the Van de Graaff staff members E.P. Knaetsch, D. Roller, and W. Seith for their help and support of the experiment especially in the preparation of the metallic Li-targets. We thank the Fonds zur Förderung der wissenschaftlichen Forschung in Österreich (project S7307-AST), the Österreichische Nationalbank (project 5054) and the Deutsche Forschungsgemeinschaft (DFG) (project Mo739/1-1) for their support.

- [1] E. M. Burbidge, G. R. Burbidge, W. A. Fowler, and F. Hoyle, *Rev. Mod. Phys.* **29**, 547 (1957).
- [2] D. G. Sandler, S. E. Koonin and W. A. Fowler, *Astrophys. J.* **259**, 908 (1982).
- [3] W. Ziegert *et al.*, *Phys. Rev. Lett.* **55**, 1935 (1985).
- [4] A. Wöhr *et al.*, in *Proceedings of the Eighth International Symposium on Gamma-Ray Spectroscopy and Related Topics, 20.-24.9. 1993, Fribourg, Switzerland*, edited by J. Kern, (World Scientific, Singapore, 1994), p. 762.
- [5] Y. Uozumi, O. Iwamoto, S. Widodo, A. Nohtomi, T. Sakae, M. Matoba, M. Nakano, T. Maki and N. Koori, *Nucl. Phys.* **A576**, 123 (1994).
- [6] R. F. Carlton, J. A. Harvey, N. W. Hill, and R. L. Macklin, in *Capture Gamma-Ray Spectroscopy and Related Topics*, edited by S. Raman, *AIP Conf. Proc.* **125**, 774 (1985).
- [7] R. F. Carlton, J. A. Harvey, R. L. Macklin, C. H. Johnson, and B. Castel, *Nucl. Phys.* **A465**, 274 (1987).
- [8] W. Ziegert, Diploma Thesis, Univ. Mainz (1980).
- [9] L. C. Carraz *et al.*, *Phys. Lett.* **109B**, 419 (1982).
- [10] W. D. Metz, W. D. Callender, and C. K. Bockelmann, *Phys. Rev. C* **12**, 827 (1975).
- [11] E. Krausmann, W. Balogh, H. Oberhummer, T. Rauscher, K.-L. Kratz, and W. Ziegert, *Phys. Rev. C* **53**, 469 (1996).
- [12] F. P. Cranston and D. H. White, *Nucl. Phys.* **A169**, 95 (1971).
- [13] F. Käppeler, G. Walter, and G. J. Mathews, *Astrophys. J.* **291**, 319 (1985).
- [14] C. Coceva, A. Brusegan, and C. Van der Vorst, *Nucl. Instr. and Meth. in Phys. Res. A*, in press.
- [15] G. Chilosi, G. D. O'Kelley, and R. Eichler, *Nucl. Phys.* **A136**, 649 (1969).
- [16] S. E. Arnell, R. Hardell, Ö. Skeppstedt, and E. Wallander, *Proc. Intern. Symp. Neutron Capture Spectroscopy*, Studsvik, IAEA, Vienna (1969), p. 231
- [17] S. F. Mughabghab, M. Divadeenam, and N. E. Holden, *Neutron Cross-sections, Vol. I* (Academic Press, 1981).
- [18] A. Owens, S. M. Pascarelle, N. Gehrels, and B. I. Teegarden, *Nucl. Instr. and Meth. in Phys. Res.* **A310**, 681 (1991).
- [19] H. Beer, G. Rupp, F. Voß, and F. Käppeler, *Nucl. Instr. Methods A* **337**, 492 (1994).
- [20] H. Beer, P. V. Sedyshev, Yu. P. Popov, W. Balogh, H. Herndl, and H. Oberhummer, *Phys. Rev. C* **52**, 3442 (1995).
- [21] H. Beer, M. Wiescher, F. Käppeler, J. Görres, and P. Koehler, *Ap. J.* **387**, 258 (1992).
- [22] E. Storm and H. Israel, *Nucl. Data Tables A* **7**, 565 (1970).
- [23] W. M. J. Veigele, *Atomic Data Nucl. Data Tables* **5**, 51 (1973).
- [24] R. L. Macklin, 1982, private communication.
- [25] W. Ratynski and F. Käppeler, *Phys. Rev. C* **37**, 595 (1988).
- [26] K. H. Kim, M. H. Park, and B. T. Kim, *Phys. Rev. C* **35**, 363 (1987).
- [27] P. Mohr, H. Abele, R. Zwiebel, G. Staudt, H. Krauss, H. Oberhummer, A. Denker, J. W. Hammer, and G. Wolf, *Phys. Rev. C* **48**, 1420 (1993).
- [28] K. Grün and H. Oberhummer, TU Wien, code TEDCA, 1995, unpublished.
- [29] H. de Vries, C. W. de Jager and C. de Vries, *At. Data Nucl. Data Tables* **36**, 495 (1987).
- [30] A. M. Kobos, B. A. Brown, R. Lindsay, and G. R. Satchler, *Nucl. Phys.* **A425**, 205 (1984).
- [31] H. Abele and G. Staudt, *Phys. Rev. C* **47**, 742 (1993).
- [32] H. Abele, University of Tübingen, code DFOLD, 1986, unpublished.
- [33] S. Raman, S. Kahane, R. M. Moon, J. A. Fernandez-Baca, J. L. Zarestky, J. E. Lynn, and J. W. Richardson, Jr., *Phys. Rev. C* **39**, 1297 (1989).
- [34] V. F. Sears, *Neutron News*, **3**, 26 (1992).
- [35] J. D. Lawson, *Phil. Mag.* **44**, 102 (1953).
- [36] J. M. Peterson, *Phys. Rev.* **125**, 955 (1962).
- [37] C. Ramsauer, *Ann. Phys.* **66**, 546 (1921).
- [38] R. L. Macklin, 1996, private communication.
- [39] F. R. Niederer *et al.*, *Geochim. Cosmochim. Acta* **48**, 1249 (1984).
- [40] C. L. Harper in *Proceedings of the 2nd International Symposium on Nuclear Astrophysics, Nuclei in the Cosmos, Karlsruhe, 6.-10. July, 1992, Karlsruhe, Germany*, edited by F. Käppeler and K. Wisshak, (IOP Publishing Ltd., London, 1993), p. 113.
- [41] B. A. Brown, A. Etchegoyen, W. D. M. Rae, and N. S. Godwin, code OXBASH, 1984 (unpublished).
- [42] W. A. Richter, M. G. van der Merwe, R. E. Julies, and B. A. Brown, *Nucl. Phys.* **A523** (1991) 325.
- [43] W. A. Fowler, G. R. Caughlan, and B. A. Zimmerman, *Ann. Rev. Astron. and Astrophys.* **5**, 525 (1967).

TABLE I. Sample characteristics and decay properties of the product nuclei ^{49}Ca and ^{198}Au

Isotope	Chemical form	Isotopic composition (%)	Reaction	$T_{1/2}$	E_γ (keV)	Intensity per decay (%)
^{48}Ca	CaCO_3	20.42(40), 0.24(42), 0.060(43), 1.48(44), 0.01(46), 77.87±1.90(48)	$^{48}\text{Ca}(n,\gamma)^{49}\text{Ca}$	(8.716±0.011) min	3084.54	92.1±1.0
^{197}Au	metallic	100	$^{197}\text{Au}(n,\gamma)^{198}\text{Au}$	2.69 d	412	95.50±0.096

TABLE II. Sample weight and experimental ^{48}Ca capture at thermal energy

Sample	Weight (mg)	Isotope	Primary ^{49}Ca Transitions			σ_{thermal} (mbarn)
			J^π	E_γ (keV)	f_γ (%)	
CaCO_3	108.630	^{48}Ca	$3/2^-$	5142	74 ± 3	982 \pm 46
			$1/2^-$	3121	23 ± 1	

 TABLE III. Sample weights and experimental ^{48}Ca capture cross-sections at thermonuclear energies

Mean neutron energy (keV)	Mass of Au front side (mg)	Mass of CaCO_3 (mg)	Mass of Au back side (mg)	Irradiation time (d)	σ (μbarn)	Uncertainty	
						statistical (%)	total (%)
25	15.577	18.28	15.583	0.98	721	1.4	10
	15.745	10.064	15.755	0.94	719	0.9	10
	15.390	21.353	15.352	0.80	767	1.4	9
	16.010	8.6025	15.950	0.86	817	1.5	10
	16.08	11.243	16.115	0.97	781	3.8	10
	15.915	7.017	15.782	0.91	733	3.4	10
	Average					751 \pm 68	
151 ± 15	15.657	49.914	15.673	1.77	331	2.1	12
	Average				331 \pm 40		
176 ± 20	15.553	70.58	15.570	3.70	303	1.5	11
	15.186	67.22	15.248	3.90	310	2.0	11
	Average				306 \pm 31		
218 ± 23	16.740	58.150	16.783	5.66	318	2.1	10
	15.482	68.790	15.532	4.07	294	1.3	10
	Average				304 \pm 31		

 TABLE IV. Final states of the reaction $^{48}\text{Ca}(n,\gamma)^{49}\text{Ca}$: J^π , excitation energies, potential parameters, and spectroscopic factors.

J^π	E^* (keV)	λ	J_R^{fold} (MeV fm 3)	V_0 (MeV)	J_R^{SW} (MeV fm 3)	$C^2 S^{\text{fold}}$	$C^2 S^{\text{SW}}$	$C^2 S_{(\text{d,p})}$ (Ref. [5])
$3/2^-$	0.0	0.9892	441.82	49.622	488.06	0.72 ± 0.04	0.73 ± 0.04	0.84 ± 0.12
$1/2^-$	2023.2	0.9111	406.92	45.639	448.89	0.86 ± 0.05	0.85 ± 0.05	0.91 ± 0.15

 TABLE V. Spins, excitation energies, Q-values and spectroscopic factors of levels in ^{49}Ca extracted from (n, γ)-data (this work), (d,p)-data [5], and the shell model (SM)

J^π	E^* [MeV]	Q [MeV]	$S_{(\text{n},\gamma)}$	$S_{(\text{d,p})}$	S_{SM}
$3/2^-$	0.000	5.142	0.72	0.84	0.91
$1/2^-$	2.023	3.121	0.86	0.91	0.94
$5/2^-$	3.586	1.556	–	0.11	–
$5/2^-$	3.993	1.149	–	0.84	0.93
$3/2^-$	4.069	1.073	–	0.13	0.01
$1/2^-$	4.261	0.881	–	0.12	–

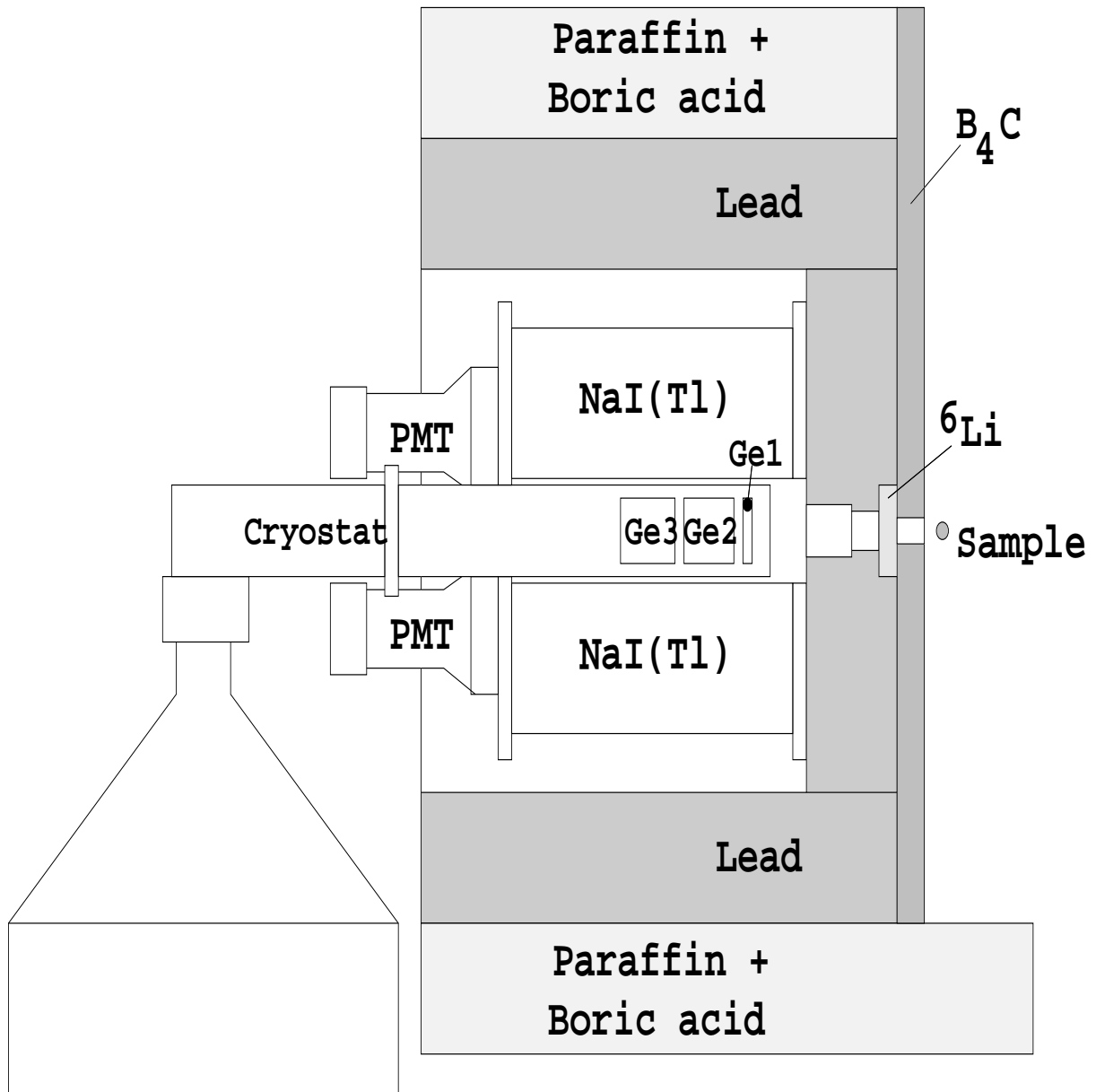


FIG. 1. Scheme of experimental setup of the thermal measurement

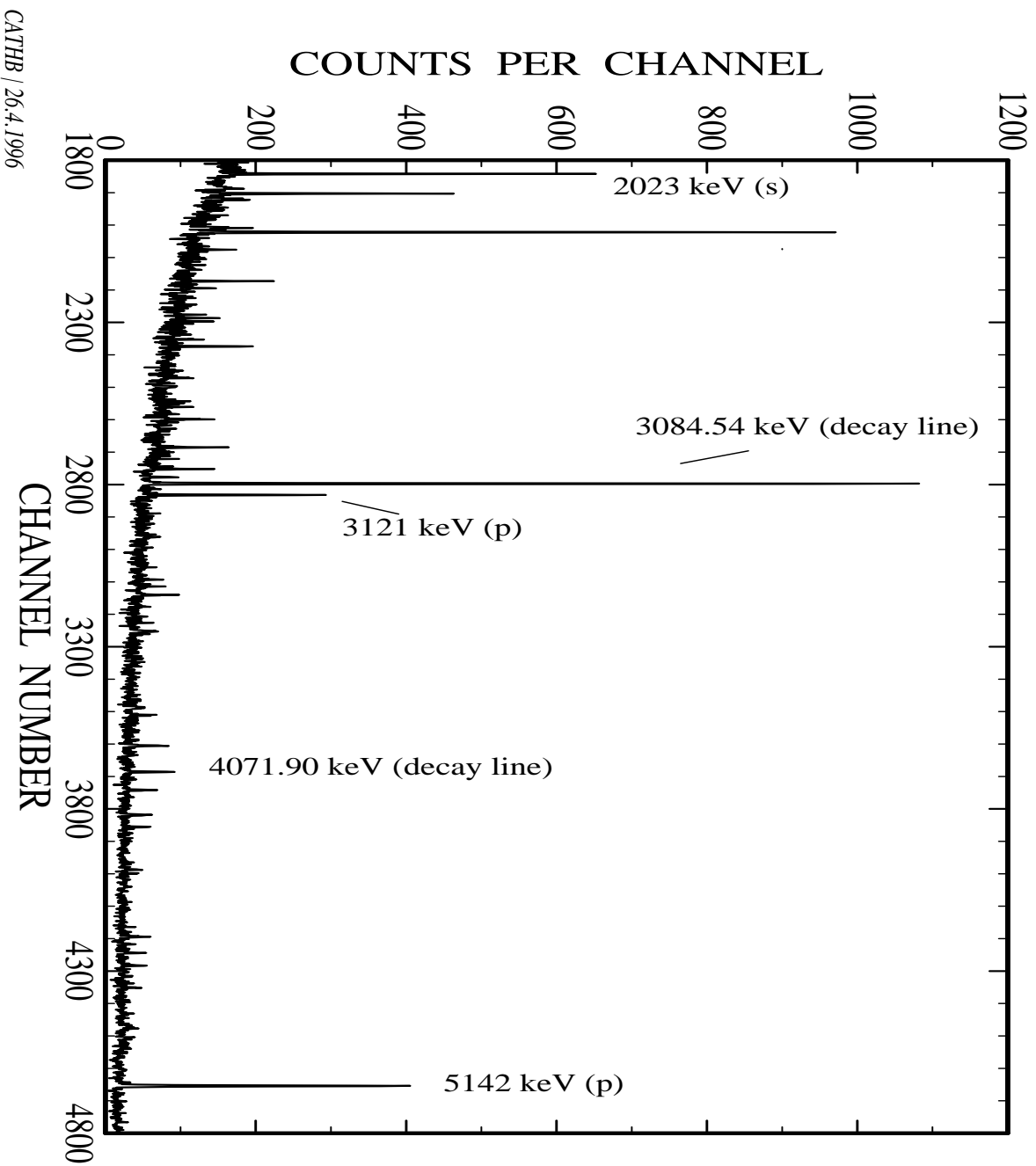


FIG. 2. Accumulated intensities of the prompt ^{49}Ca and β -delayed ^{49}Sc γ -lines from the thermal experiment

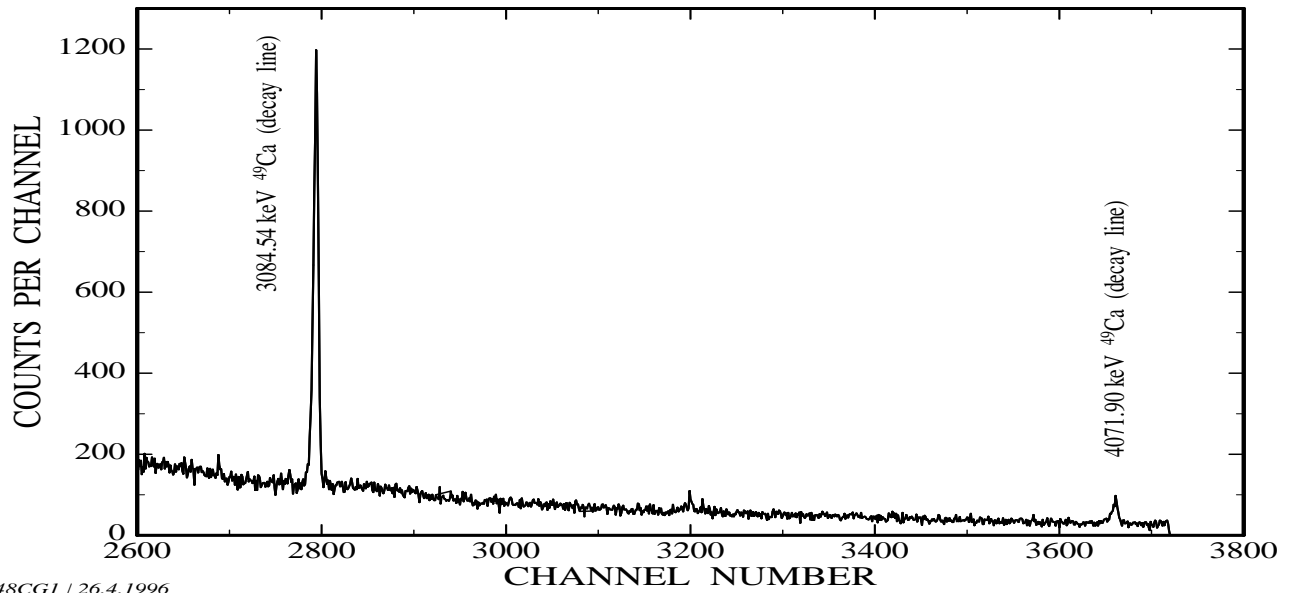
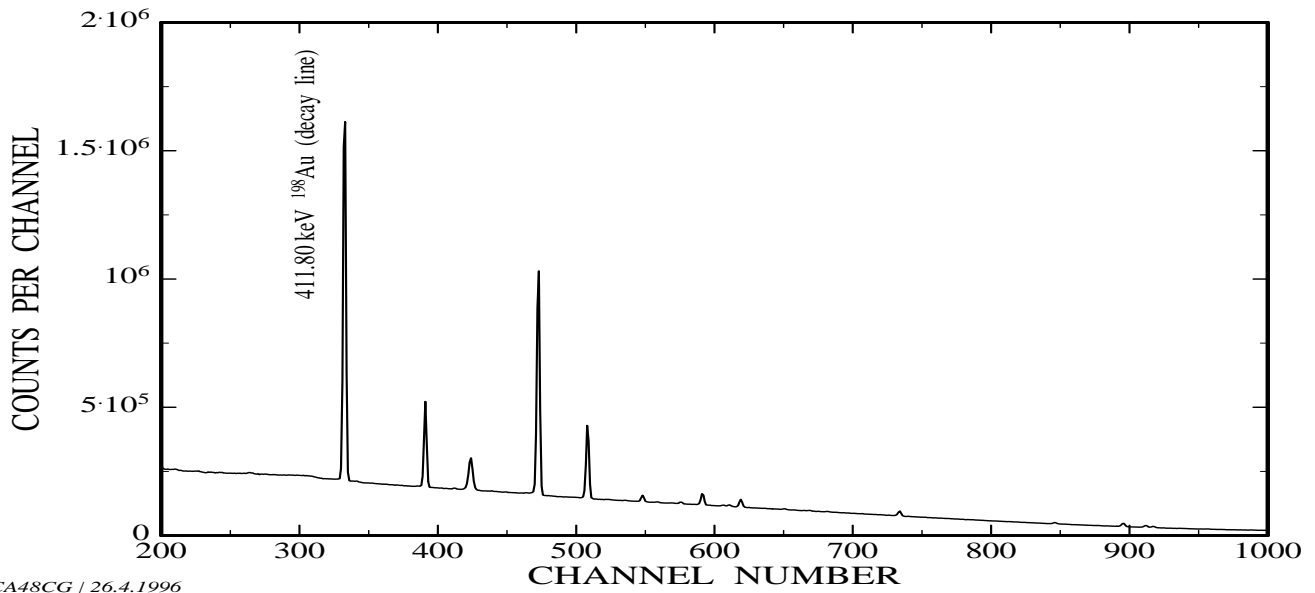


FIG. 3. Accumulated intensities of the ^{49}Ca (below) and ^{198}Au (above) γ -ray decay lines from the activation with a 50.40 mg CaCO_3 sample sandwiched by two Au foils using a neutron spectrum with a mean energy of 176 keV

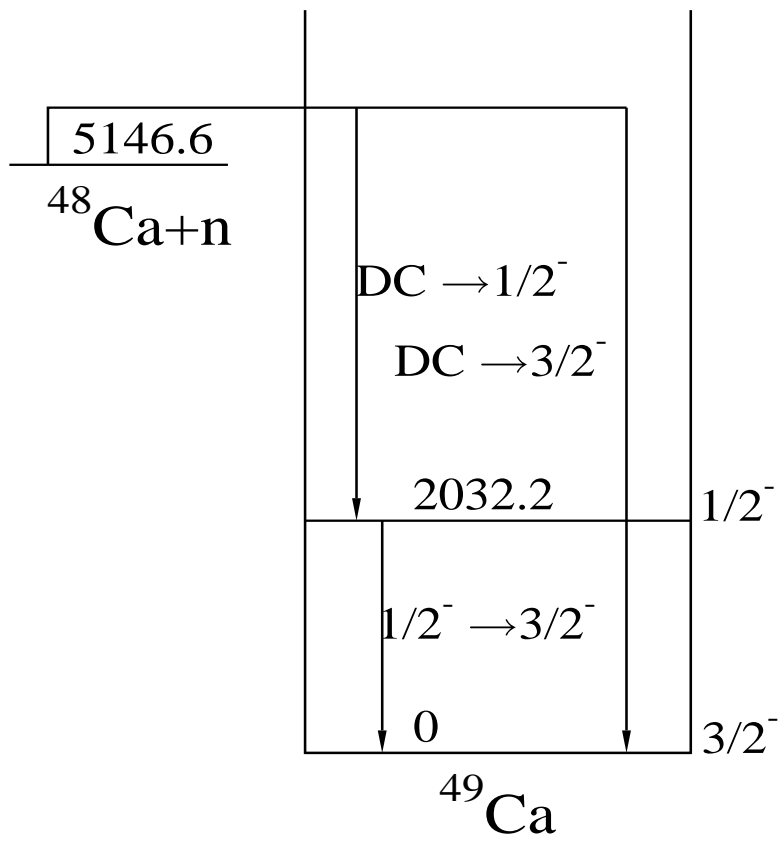


FIG. 4. Partial level scheme of ^{49}Ca

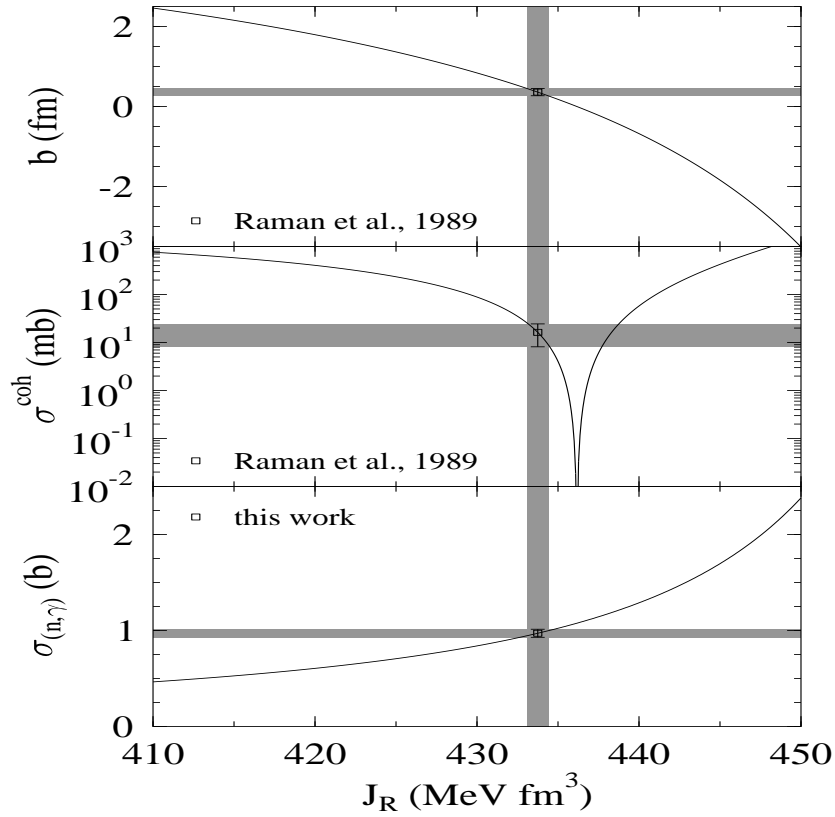


FIG. 5. Neutron scattering length b , coherent elastic scattering cross section σ^{coh} , and thermal capture cross-section (and their uncertainties, gray shaded) in dependence of the volume integral of the folding potential: the potential strength can be adjusted very accurately because of the very small scattering length which is close to zero.

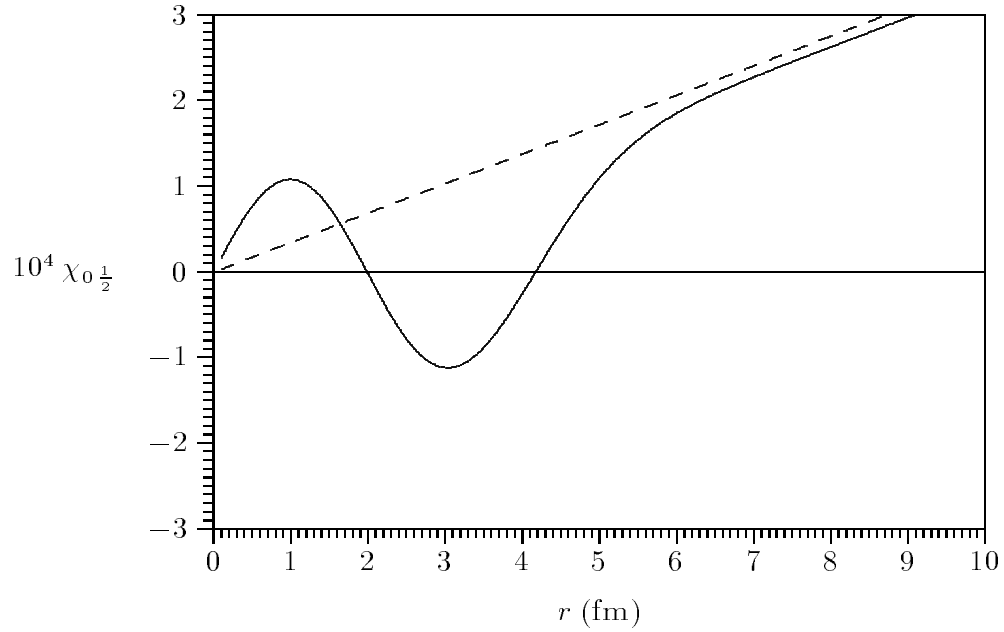


FIG. 6. Real part of the ($^{48}\text{Ca}+n$)-scattering wave function $\chi_{\ell=0, j=1/2}$ using a folding potential fitted to the experimental scattering cross section (solid curve), and for a vanishing potential (dashed curve)

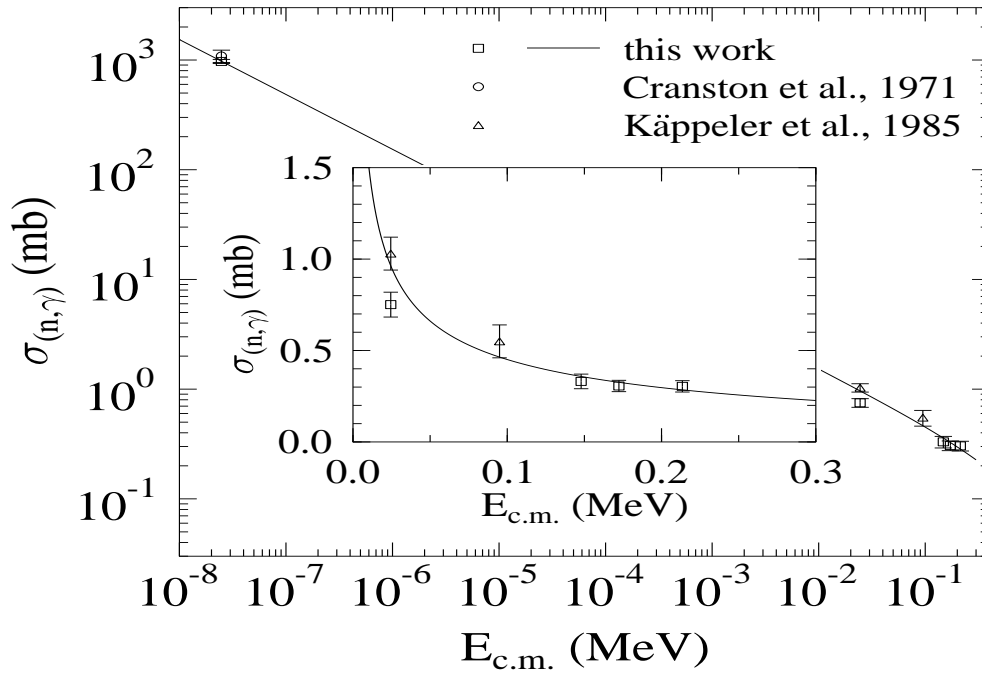
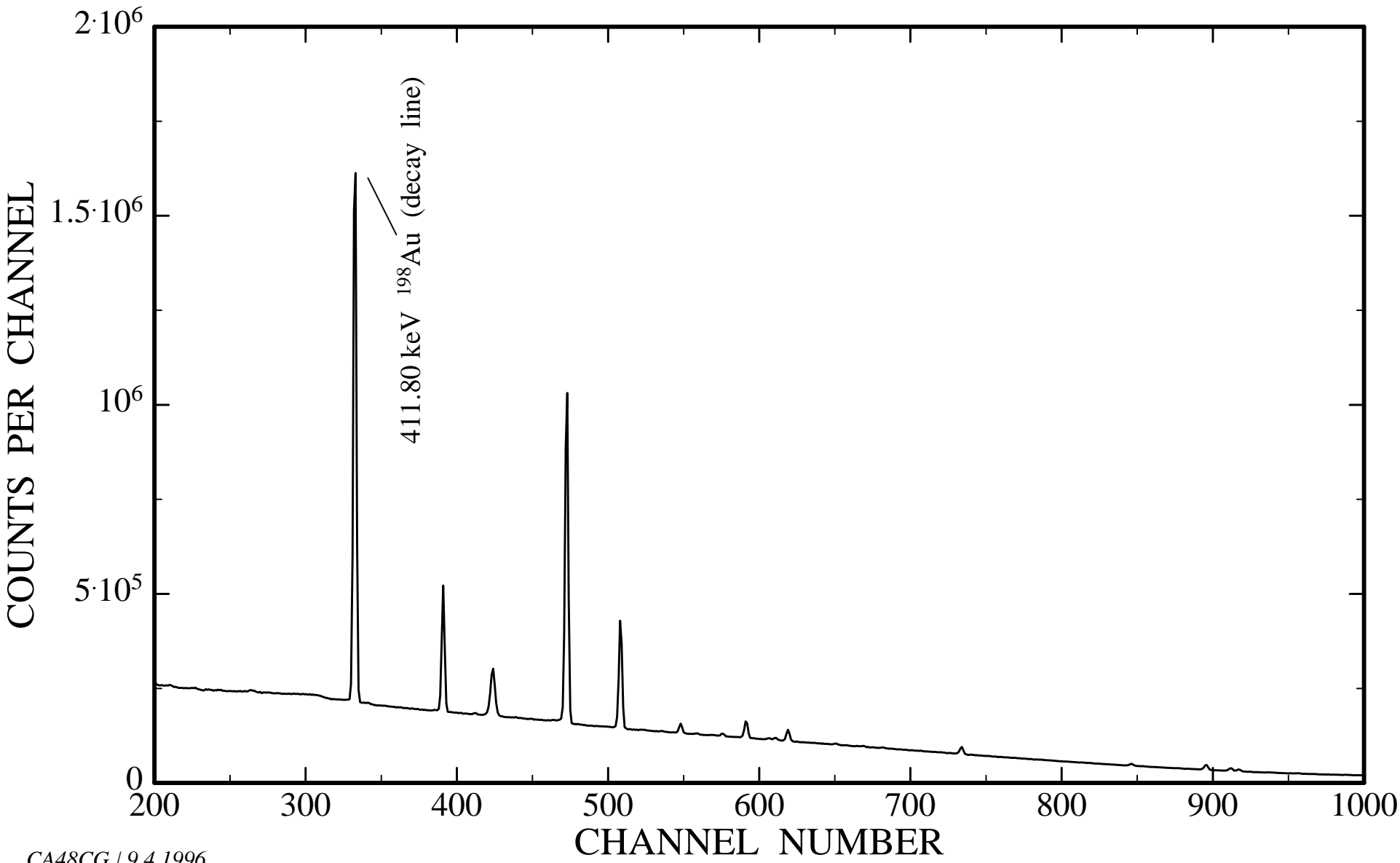


FIG. 7. Comparison of the direct-capture cross-section for $^{48}\text{Ca}(n,\gamma)^{49}\text{Ca}$ at thermal and thermonuclear energies with the experimental data



CA48CG / 9.4.1996